Inorganic Chemistry

pubs.acs.org/IC Article

Spontaneous Formation of an Fe/Mn Diamond Core: Models for the Fe/Mn Sites in Class 1c Ribonucleotide Reductases

Patrick M. Crossland, Yisong Guo,* and Lawrence Que, Jr.

Cite This: https://doi.org/10.1021/acs.inorgchem.1c00684 Read Online

ABSTRACT: A handful of oxygen-activating enzymes has recently been found to contain Fe/Mn active sites, like Class 1c ribonucleotide reductases and R2-like ligand-binding oxidase, which are closely related to their better characterized diiron cousins. These enzymes are proposed to form high-valent intermediates with Fe−O−Mn cores. Herein, we report the first examples of synthetic Fe/Mn complexes that mimic doubly bridged intermediates proposed for enzymatic oxygen activation. Fe K-edge extended X-ray absorption fine structure (EXAFS) analysis has been used to characterize the structures of each of these compounds. Linear compounds accurately model the Fe···Mn distances found in Fe/Mn proteins in their resting states, and doubly bridged diamond core compounds accurately model the distances found in high-valent biological intermediates. Unlike their diiron analogues, the paramagnetic nature of Fe/Mn compounds can be analyzed by EPR, revealing $S = 1/2$ signals that reflect antiferromagnetic coupling between the high-spin Fe(III) and Mn(III) units of heterobimetallic centers. These compounds undergo electron transfer with various ferrocenes, linear compounds being capable of oxidizing diacetyl ferrocene, a weak reductant, and diamond core compounds being capable of oxidizing acetyl ferrocene. Diamond core compounds can also perform HAT reactions from substrates with X−H bonds with bond dissociation free energies (BDFEs) up to 75 kcal/mol and are capable of oxidizing TEMPO-H at rates of 0.32−0.37 M^{-1} s^{-1}, which are comparable to those reported for some mononuclear Fe^{III}−OH and Mn^{III}−OH compounds. However, such reactivity is not observed for the corresponding diiron compounds, a difference that Nature may have taken advantage of in evolving enzymes with heterobimetallic active sites.

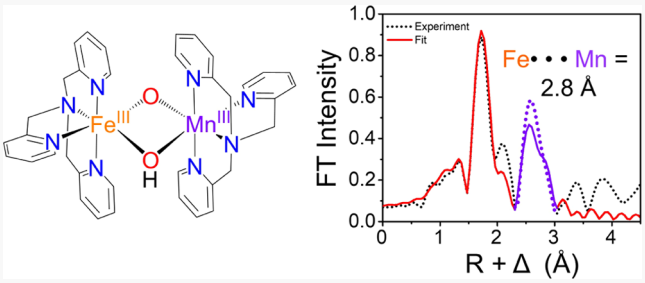

■ INTRODUCTION

In Nature, oxygen activation, reduction, and formation are performed at a variety of metallo-cofactors and active sites. These include mono- and diiron sites,[1,2] mono- and dicopper sites,[3] the CaO_5Mn_4 oxygen-evolving complex,[4] and the iron−copper active site of heme-copper oxidases.[5] In the past 15 years, two more proteins with heterobimetallic sites that activate oxygen have been discovered.[6,7] Ribonucleotide reductase 1c (RNR1c) is found in the human pathogen *Chlamydia trachomatis* and is responsible for reducing RNA to DNA.[6,8,9] R2-like ligand-binding oxidase (R2lox) is found in the human pathogen *Mycobacterium tuberculosis* and while its function is currently unknown, it has been correlated with virulence.[7]

These two enzymes are proposed to follow analogous mechanisms of oxygen activation. O_2 binds to a Fe^{II}/Mn^{II} site to form an Fe^{III}/Mn^{III}−peroxy intermediate.[10] The O−O bond is then cleaved to form high-valent Fe^{IV}/Mn^{IV} intermediates with bis-μ-O^{2-} "diamond core" moieties.[10−12] In RNR1c, this high-valent intermediate is then reduced by one electron and protonated to form a $Fe^{III}(\mu\text{-O})(\mu\text{-OH})Mn^{IV}$ intermediate that is responsible for initiating the radical translocation that forms the catalytically active thiyl radical.[9,13,14] In contrast, the proposed high-valent intermediate in R2lox performs a two-electron oxidation on the protein scaffold and forms an ether cross-link between valine and tyrosine residues.[10,15]

In other biological systems that utilize high-valent metals, synthetic mimics have been helpful for understanding the structure and reactivity of short-lived biological intermediates. While much work has been done synthetically for mono- and diiron systems,[2,16] the OEC,[17] and mono- and dicopper systems,[18] currently there has been little work done to model RNR1c and R2lox.

Early synthetic work on Fe/Mn compounds was performed by Wieghardt et al. who were interested in the physical and electronic structures of heterobimetallic complexes. These complexes were formed by self-assembly following the hydrolysis of a 1:1 mixture of $FeCl_3$(TACN) (TACN =

Received: March 5, 2021

1,4,7-triazacyclononane) and $MnCl_3(Me_3TACN)$ (Me_3TACN = 1,4,7-trimethyl-1,4,7-triazacyclonane) in the presence of sodium acetate, resulting in the formation of $[(TACN)Fe(\mu\text{-}O)(\mu\text{-}OAc)_2Mn(Me_3TACN)]^{2+}$.[19]

Early synthetic efforts of Que and co-workers used the symmetric dinucleating ligand BPMP (BPMP = 2,6-bis[(bis(2-pyridylmethyl)-amino)methyl]-4-methylphenolate) to form Fe^{III}/Mn^{II} complexes in an effort to model purple acid phosphatase (PAP) active sites.[20] These efforts were followed up more recently by Latour and Nordlander, who used unsymmetric dinucleating ligands to incorporate the open coordination site on the Mn ion found in PAP.[21,22]

While previously studied systems have effectively modeled the PAP active site, none had an open coordination site on each metal that would allow the structures proposed in RNR1c and R2lox to be effectively modeled. To this end, we have demonstrated that the reaction of a high-valent $Fe^{IV}(O)$ compound with Mn^{II} complexes forms the oxo-bridged Fe^{III}–O–Mn^{III} products.[23] One of these complexes, $[(TPA)(solv)Fe^{III}(\mu\text{-}O)Mn^{III}(solv)(TPA)]^{4+}$, was shown to be able to bind exogenous ligands such as acetate. We now also show that three linear $[(L)(solv)Fe^{III}(\mu\text{-}O)\ Mn^{III}(solv)(L')]$ (L = tris(pyridin-2-ylmethyl)amine, TPA, tris((5-methylpyridin-2-yl)methyl)amine, $5Me_3TPA$, or 1-(4-methoxy-3,5-dimethylpyridin-2-yl)-*N*-((4-methoxy-3,5-dimethylpyridin-2-yl)-methyl)-*N*-((5-methoxy-4,6-dimethylpyridin-2-yl)methyl)-methanamine, TPA*; L′ = TPA) complexes can be converted to their respective conjugate bases $[(L)Fe^{III}(\mu\text{-}O)(\mu\text{-}OH)Mn^{III}(L)]^{3+}$ by the addition of 1 equiv of base, representing the first synthesis of such compounds. Depending on the supporting ligand on ferric ion, the strength of the base required to fully convert the linear compound to doubly bridged complex changes, which allows for the pK_a of each compound to be determined. In sharp contrast to the corresponding diiron complexes, the Fe/Mn compounds spontaneously form $Fe(\mu\text{-}O)(\mu\text{-}OH)Mn$ diamond cores in the presence of excess water, a unique result that highlights the difference between homo- and heterobimetallic complexes. These Fe/Mn compounds also exhibit electron transfer and hydrogen atom transfer reactivity that is unobserved in diferric complexes (Scheme 1).

■ RESULTS AND DISCUSSION

As previously reported, the formation of $(L)Fe^{III}$–O–$Mn^{III}(L)$ complexes can be achieved by the reaction of the appropriate ferryl species, generated in situ from the reaction of an Fe^{II} precursor and an iodosyl arene, and a Mn^{II} precursor.[23] In the interest of expanding this library of compounds and investigating ligand effects on their properties, two variants of the parent $[(TPA)(solv)Fe^{III}$–O–$Mn^{III}(solv)(TPA)]^{4+}$ (**1**) complex have been synthesized by the same method, namely $[(5Me_3TPA)(solv)Fe^{III}$–O–$Mn^{III}(solv)(TPA)]^{4+}$ (**2**) and $[(TPA^*)(solv)Fe^{III}$–O–$Mn^{III}(solv)(TPA)]^{4+}$ (**3**). The UV–vis spectra of these compounds are similar, each with a sharper feature at ∼500 nm, and a broader feature at ∼550 nm (Figure S1). The shape of this second feature seems to vary between the compounds, but the basis for these relatively minor differences is not currently established.

Upon titration of **1**, **2**, or **3** with triethylamine, a strong base in acetonitrile (pK_a in MeCN = 18.82), a new species is observed to form with λ_{max} = 455 nm. This species maximally forms upon the addition of 1 equiv of TEA and is designated **1-OH**, **2-OH**, or **3-OH**, respectively, the conjugate bases of **1**, **2**, or **3** (Figure 1, top). Further addition of base causes these conjugate base complexes to decay. On the other hand, the

Scheme 1. Spontaneous Formation of a Complex with an Fe^{III}/Mn^{III} Diamond Core upon Addition of Water

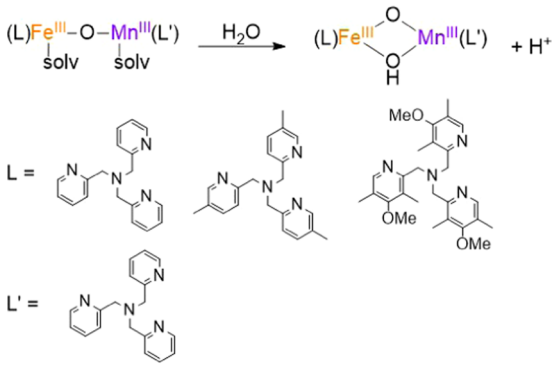

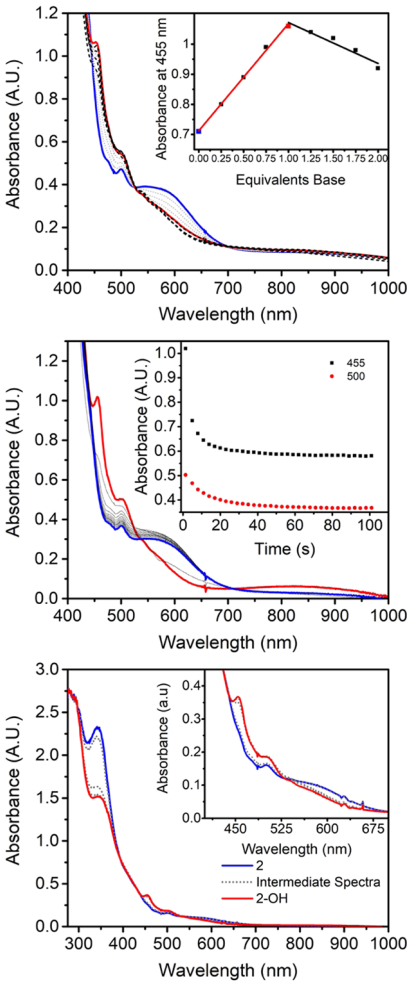

Figure 1. Top: Titration of **2** (blue) with TEA in MeCN at −40 °C to form **2-OH** (red) and the decay of **2-OH** upon the addition of excess TEA (dotted black). Middle: Addition of $HClO_4$ to **2-OH** (red) to regenerate **2** (blue). The intermediate spectra have higher absorbance than **2** because the mixing time is close to the half-life of the reaction. Bottom: Spectra of 1 mM **2** (blue) in a 0.5 cm pathlength cuvette and its conversion to **2-OH** upon base addition (red). The change in intensity of the 350 nm feature indicates that it is associated with **2**.

https://doi.org/10.1021/acs.inorgchem.1c00684
Inorg. Chem. XXXX, XXX, XXX−XXX

addition of 1 equiv of acid to **1-OH**, **2-OH**, or **3-OH** fully converts these species back to **1**, **2**, or **3**, respectively.

The UV−vis features associated with all six complexes persist at −40 °C for several hours and are clearly different from those of related homobimetallic complexes.[24,25] Unfortunately, attempts at crystallization of these heterobimetallic complexes have only yielded homodinuclear complexes, as it takes several days to obtain crystals. Fortunately, electron paramagnetic resonance (EPR) spectroscopy provides strong evidence for the heterobimetallic nature of the resulting complexes.

The X-band EPR spectra of **1**, **2**, **1-OH**, and **2-OH** all show signals near $g = 2$, indicative of an $S = 1/2$ species arising from an antiferromagnetically coupled high-spin Fe^{III} and Mn^{III} pair (Figure 2). This signal shows a six-line pattern arising from

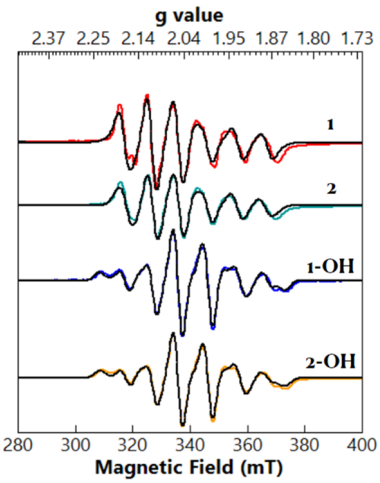

Figure 2. EPR spectra of **1**, **2**, **1-OH**, and **2-OH** in MeCN. Actual data are colored, while simulations are shown in black. Simulation parameters are listed in Table 1.

hyperfine splitting from the I = 5/2 Mn^{III} ion in the complex. Spin quantification using $Cu(ClO4)_2$ as a standard shows that **1**, **1-OH**, **2**, and **2-OH** are all formed in greater than 90% yield. Complexes **1** and **2** exhibit respective axial EPR signals with g values of 2.039, 2.015, 2.015 and g = 2.038, 2.015, 2.015 and ^{55}Mn nuclear hyperfine coupling of different magnitudes along the three principal axes (Table 1). In contrast, **1-OH** and **2-OH** exhibit rhombic EPR signals, with g = 2.03, 2.022, 2.015 and g = 2.030, 2.027, and 2.014, respectively, and ^{55}Mn hyperfine splittings different from those of **1** and **2** (Table 1). These signals are also clearly distinct from the starting Mn^{II} complex, which is best simulated with a rhombic, $S = 5/2$ signal (Table 1 and Figure S13). No additional ^{1}H super-

Table 1. Comparison of the EPR Parameters Observed for Synthetic and Biological Fe/Mn Centers

complex	g	A_{Mn}
1	2.039, 2.015	190, 287, 313
2	2.038, 2.015	190, 270, 311
1-OH	2.030, 2.022, 2.015	209, 368, 280
2-OH	2.030, 2.027, 2.014	200, 370, 277
$(TPA)Mn^{II}(OTf)_2$	2.02, 2.01, 1.98	268, 253, 248
Mt R2lox[26]	2.034, 1.968, 1.953	282, 249, 257
RNR 1c $Fe^{IV}(\mu\text{-}O)_2Mn^{IV}$[12]	2.028, 2.021, 2.013	221, 243, 246

hyperfine splitting is observed in the complexes with hydroxo bridges, nor are the EPR signals affected upon deuteration of the hydroxo bridges. (Figure S10).

Comparison of the EPR spectra of the reported complexes to those of related biological intermediates shows that the synthetic compounds are able to model some aspects of the electronic structures of the corresponding biological species. The g tensor of the resting state of *Mt*R2lox, which has a singly bridged Fe^{III}/Mn^{III} center, is rhombic, in contrast to the axial signals found for **1** and **2**. However, both **1** and **2** as well as R2lox show clear evidence for ^{55}Mn nuclear hyperfine splitting along all three principal axes. Besides differences between histidine and carboxylate ligands found in enzyme active sites vs the pyridine/amine donor combination in synthetic complexes, the $Fe-O_{bridge}$ distance reported for R2lox is 2.1 Å, significantly longer than $Fe/Mn-O_{bridge}$ distances found in **1** and **2** (vide infra). This M···M′ distance suggests that the bridging ligand in R2lox is not an oxo group, but rather a protonated derivative thereof.[15]

Perhaps unexpectedly, **1-OH** and **2-OH** exhibit EPR signals that strongly resemble those of biological Fe/Mn diamond cores, despite the fact that the signals associated with the latter correspond to the trapped high-valent intermediate for RNR 1c, which has been shown to have an $Fe^{IV}(\mu\text{-}O)_2Mn^{IV}$ center. The differences in oxidation state and bridging ligand do not appear to affect the g values for this set of compounds. The Mn^{III} ion is most likely in the high-spin state in **1-OH** and **2-OH** as well as in RNR 1c. For mononuclear high-spin Mn complexes, Mn^{II}, Mn^{III}, and Mn^{IV} complexes all exhibit small g anisotropy with g values that do not vary much from $g = 2$.[27] Similarly, high-spin ferric ions also exhibit an isotropic g tensor with values close to 2. Even for the few mononuclear high-spin Fe^{IV} species reported, the g values do not significantly deviate from 2.[28,29] Therefore, Fe/Mn diamond cores that generally exhibit strong antiferromagnetic coupling interactions between the two metal ions, such as **1-OH**, **2-OH**, and the RNR 1c $Fe^{IV}(\mu\text{-}O)_2Mn^{IV}$ center have g values in the coupled system that are all close to 2. The biggest differences arise in the hyperfine splitting, where $A_{Mn(y)}$ is much larger for synthetic complexes. The reasons for this pattern are unclear and beyond the scope of this work, but these results clearly illustrate that synthetic models can be useful for mimicking the electronic structures of their biological cousins.

Similar to well-established diiron precedents,[30−32] resonance Raman studies of six Fe−O−Mn complexes in this study show Fe−O−Mn vibrations that are sensitive to the Fe−O−Mn angle.[2,23,30] The resonance Raman spectra of **1**−**3** obtained at 77 or 233 K with 405 nm excitation (Figures 3, S6 and Table 1) show resonance-enhanced features at 853−862 cm^{-1}, corresponding to the asymmetric Fe−O−Mn vibration. In the case of **1**, a Fermi doublet centered at 854 cm^{-1} is observed at 861 and 848 cm^{-1}. Issues encountered with sample fluorescence in the case of **2** required experiments to be performed in a liquid solution at 233 K. The strong enhancement of vibrations associated with **1** using 405 nm excitation suggests that these Fe−O−Mn complexes have oxo-to-M(III) ligand-to-metal charge-transfer (LMCT) bands in the near-UV region. Indeed, the UV−vis spectra of **1**, **2**, and **3** reveal strong absorptions near 350 nm (Figure 1 and Table 2), which decrease intensity upon conversion to **1-OH**, **2-OH**, and **3-OH**, respectively (Figures 1 and S3).

Essentially identical resonance Raman spectra with features at 651 and 611 cm^{-1} are obtained for **1-OH**, **2-OH**, and **3-OH**

https://doi.org/10.1021/acs.inorgchem.1c00684
Inorg. Chem. XXXX, XXX, XXX−XXX

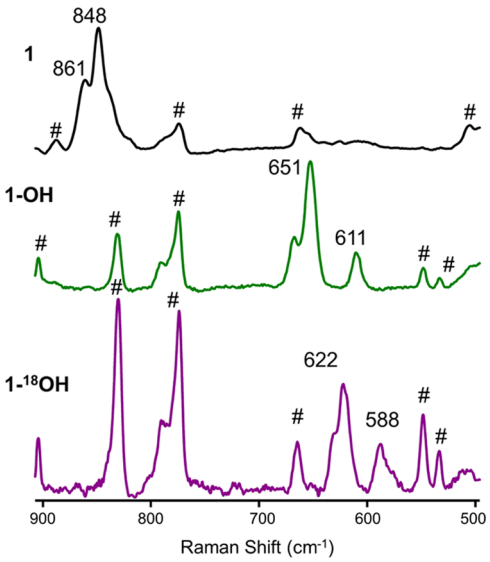

Figure 3. Resonance Raman data obtained at 77 K for 1 mM **1** in MeCN with 405 nm excitation and for 1 mM **1-OH** in MeCN with 457 nm excitation. # denotes solvent peaks.

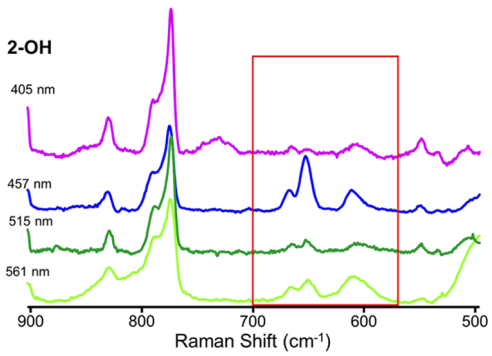

Figure 4. Excitation profile of **2-OH** in MeCN at four different laser wavelengths. The signal is most enhanced with excitation at 457 nm, very close to the charge-transfer band observed in its visible spectrum. The red box highlights Fe−O−Mn vibrations of interest.

with 457 nm excitation (Figures 3 and S6). Based on Raman data for (μ-oxo)diiron complexes,[33] vibrations in this region are indicative of rather acute Fe−O−Fe angles approaching 90°, which are characteristic of compounds with $M_2(\mu\text{-O})_2$[34−39] or $M_2(\mu\text{-O})(\mu\text{-OH})$[24,25,33] cores. The stoichiometry observed for the conversion between **1**, **2**, and **3** to their respective conjugate bases shows that forming any potential diamond core species is a one-proton equilibrium. For this reason, we assign **1-OH**, **2-OH**, and **3-OH** as having M(μ-O)(μ-OH)M′ diamond cores.

The excitation profiles of all six compounds allow us to assign the oxo-to-M^{3+} charge-transfer band for linear and doubly bridged compounds (Figures 4 and S7). Not surprisingly, vibrations for **1**, **2** and **3** are most enhanced with 405 nm excitation and likely associated with the intense 350 nm absorption band, a spectral feature, typically assigned to oxo-to-M^{3+} charge-transfer bands in Fe^{III}−O−Fe^{III} complexes.[32,38] On the other hand, **1-OH**, **2-OH**, and **3-OH** show the strongest enhancement of 651 and 611 cm^{-1} vibrations with 457 nm excitation, suggesting that the 455 nm feature may be assigned to an oxo-to-M^{3+} charge-transfer band for diamond core complexes.

To verify that these vibrations derived from an oxo moiety, $H_2{}^{18}O$ was added to a solution of **2**. The UV−vis spectrum of **2** in the presence of 200 equiv of water resembled that of **2-OH** (Figure S4), and the resonance Raman spectrum of this species indeed revealed the vibrations at 651 and 611 cm^{-1} to be sensitive to ^{18}O substitution, showing a downshift of ∼30 cm^{-1} (Figure S9). Furthermore, the vibration at 853 cm^{-1} from **2** had disappeared. These results indicate that the 853 cm^{-1} vibration belongs to one species, most likely **2**, while the vibrations at 651 and 611 cm^{-1} belong to a different species that is formed from **2** in the presence of excess water (**2-OH**). Given the labeling results, we assign ∼850 cm^{-1} vibrations to the asymmetric Fe−O−Mn mode of a nearly linear Fe−O−M moiety, consistent with results from diiron and other heterobimetallic complexes.[23,24,30] The two vibrations of comparable frequency associated with diamond core moieties

Table 2. UV−Vis and Vibrational Features of Fe−O−Mn and Related Diferric Complexes

compound	λ_{max} (nm) (ε, M^{-1} cm^{-1})	ν(Fe−O−M) (cm^{-1})[a]	λ_{exc} (nm)	refs
	Synthetic Fe/Mn Compounds			
1	350 (4600) 500 (500)	854	405	c
2	350 (4600) 500 (500)	853, 862[c]	405	c
3	350 (4600) 500 (500)	856	405	c
1-OH	455 (1000)	651, 611	457	c
2-OH	455 (1000)	651, 611	457	c
3-OH	455 (1000)	651, 611	457	c
$[(N4Py)Fe^{III}-O-Mn^{III}(dpaq)]^{3+}$	440	846	515	23
	$Fe_2{}^{III}(\mu\text{-O})(\mu\text{-O}_2H_3)$ Complexes			
TPA	322, 360 480, 610			24
5Et$_3$TPA	360, 485 605	462		24
BPEEN	320, 365 480, 650	448		24
	$Fe_2{}^{III}(\mu\text{-O})(\mu\text{-OH})$ Complexes			
TPA*	370, 550			25
6Me$_3$TPA	340, 396, 550	675	514.5	24
BQPA	308, 396, 554	668	514.5	24
BPEEN	378, 430 475, 510, 558			24
BPMEN	377, 430 479, 512, 555			24

[a]Data from frozen MeCN solutions at 77 K unless otherwise noted. [b]This work. [c]Data from liquid MeCN solution at 233 K.

https://doi.org/10.1021/acs.inorgchem.1c00684
Inorg. Chem. XXXX, XXX, XXX−XXX

can be, respectively, assigned as the asymmetric and symmetric Fe−O−Mn vibrations.[33] The more intense feature has been assigned as the asymmetric vibration, following the pattern found for (μ-oxo)diiron complexes, which provides a precedent for the metal-site inequivalence leading to a greater enhancement of the ν_{asym} mode at 651 cm^{-1} than the ν_{symm} mode at 611 cm^{-1}.[32]

These results also show that the presence of excess water converts the Fe/Mn open-core complex **2** spontaneously to the closed-core complex **2-OH**. Resonance Raman spectra of **1** and **2** formed in wet acetonitrile (Figure S8) show a mixture of the open and closed-core compounds, lending further support to the notion that Fe/Mn diamond cores spontaneously form from the open-core complexes in the presence of water. Thus, water is a strong enough base to deprotonate metal-bound water and generate the oxo-hydroxo diamond core in **2-OH**.

Complexes **1-OH**, **2-OH**, and **3-OH** differ in their Raman properties from those of diiron complexes. Based on the few $Fe_2^{III}(\mu\text{-O})(\mu\text{-OH})$ complexes reported, the latter exhibit vibrations at somewhat higher values (Table 2) and are not observed in the present study. It should also be noted that $Fe_2^{III}(\mu\text{-O})(\mu\text{-OH})$ compounds have been shown to bind water to form $Fe_2^{III}(\mu\text{-O})(\mu\text{-}H_3O_2)$ complexes under similar conditions to those which generate **1-OH**, **2-OH**, and **3-OH**.[24,25]

To further elucidate the structures of these compounds, Fe K-edge X-ray absorption spectroscopic (XAS) analysis was performed on these complexes. The X-ray absorption near-edge spectra (XANES) displayed by all six complexes are typical of high-spin ferric compounds (Figures S10 and S11), with K-edge energies in the range of 7123.6−7124.4 eV (Table S1). The pre-edge features are best fit with two components with areas totaling between 8.7 and 10.3 units, indicative of the relatively high symmetry around the Fe^{III} ion.[40]

Fe K-edge, extended X-ray absorption fine structure (EXAFS) analysis corroborates the conclusions derived from the resonance Raman data. The EXAFS spectra for **1**, **2**, and **3** all exhibit an intense peak near $R + \Delta \sim 3.5$ Å that arises from a heavy-atom scatterer (Figures 5 and S12). Given the EPR results that show heterobimetallic complexes to be formed in >90% yield, this scatterer is most likely Mn. Complexes **1**, **2**, and **3** have Fe···Mn distances of 3.63−3.65 Å, corresponding to a nearly linear Fe−O−Mn unit. All three compounds have primary coordination spheres typical of oxo-bridged high-spin diferric compounds, with an O scatterer at 1.81−1.84 Å and 5 N/O scatterers at 2.12−2.14 Å.[24,25,38,41]

In contrast, Fe K-edge EXAFS analysis of **1-OH**, **2-OH**, and **3-OH** shows a dramatic contraction of the Fe···Mn distances to ∼2.8 Å, indicative of a significant bending of the Fe−O−Mn unit to form a diamond core.[39] This contraction is noticeable in the Fourier transformed EXAFS spectra, where the Mn scatterer is now found below $R + \Delta = 3$ Å (Figures 5 and S12). Like the corresponding open-core compounds, **1-OH**, **2-OH**, and **3-OH** exhibit primary coordination sphere features of high-spin ferric compounds. Both **1-OH** and **2-OH** have Fe−O scatterers at 1.83 and 1.99 Å, which, respectively, correspond to typical bond lengths for Fe^{III}-μ-O and Fe^{III}-μ-OH units.[24,42] In contrast, **3-OH** is the best fit with one shell with two O scatterers at 1.89 Å, suggesting that the Fe−O and Fe−OH distances in this complex differ by less than 0.12 Å, the limit of the resolution for these data. Taken together, these results lend support to our assignment of **1-OH**, **2-OH**, and **3-OH** as Fe(μ-O)(μ-OH)Mn complexes.

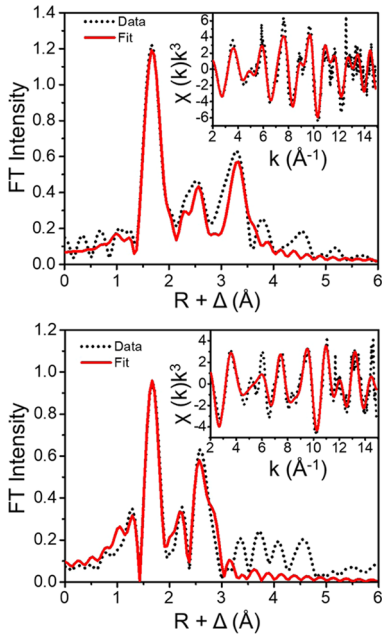

Figure 5. Top: *k*-space (inset) and Fourier transformed EXAFS data for **1** (black dots) and best fit (solid red). Bottom: *k*-space (inset) and Fourier transformed EXAFS data for **1-OH** (black dots) and best fit (solid red).

The observed Fe···Mn distances in **1-OH**, **2-OH**, and **3-OH** are comparable to those found for $Fe_2^{III}(\mu\text{-O})(\mu\text{-OH})$ complexes supported by TPA* and BPEEN ligands (Table 3). These ligands are similar to those used in the current study, with amine and pyridine-based donors with no α substituents on pyridines.[24,25] In contrast, $Fe_2^{III}(\mu\text{-O})(\mu\text{-OH})$ complexes supported by $6Me_3TPA$ and BQPA (Table 3) have longer Fe··· Fe distances.[24] We attribute this outcome to greater steric interactions imparted by the introduction of α-substituents on the pyridine moieties of $6Me_3TPA$ ligand and quinolines on the BQPA ligand—steric factors not shared by the Fe/Mn compounds in the present study.

When the structures of the synthetic complexes reported herein are compared to those of biological intermediates, it is clear that metal−metal distances reported for **1-OH**, **2-OH**, and **3-OH** are comparable to the two found in biological Fe/Mn intermediates,[12,43] despite differences in metal oxidation states. Indeed, synthetic diiron examples show that there is only a variation of around 0.2 Å in the metal−metal distances among diamond core complexes in three different oxidation states ($Fe^{III}Fe^{III}$, $Fe^{III}Fe^{IV}$, and $Fe^{IV}Fe^{IV}$).[24,25,36,37,44] These results on synthetic $Fe^{III}Mn^{III}$ complexes provide the first confirmation that such structures can exist and provide a structural basis to better understand these fleeting biological intermediates.

The EXAFS analysis results presented here for **1**−**3** differ from that reported earlier for **1**,[23] for which an Fe···Mn distance of 3.34 Å was deduced. We note that the features in the 3 Å region are better resolved in our more recent data, suggesting that the earlier sample of **1** may be a mixture of **1** and **1-OH**, a notion not considered previously as the latter complex had not yet been identified at that time. In the current study, the peak of the Mn scatterer is observed at an $R + \Delta$ value > 3 Å for **1**, as expected for a nearly linear Fe−O−Mn unit. The latter observation is corroborated by the data reported for **2** and **3** (Figure S12). On the other hand, EXAFS

https://doi.org/10.1021/acs.inorgchem.1c00684
Inorg. Chem. XXXX, XXX, XXX−XXX

Table 3. Structural Properties of Synthetic Fe/Mn Compounds and Their Biological and Diferric Analogues

synthetic Fe/Mn compounds[a]					
	Fe−O	Fe−N (ave)	Fe−O(H)	Fe−M	refs
1	1.81	2.13		3.65	this work
2	1.82	2.14		3.63	this work
3	1.84	2.12		3.64	this work
1-OH	1.82	2.14	1.99	2.79	this work
2-OH	1.84	2.15	1.99	2.77	this work
3-OH	1.89	2.10	1.89	2.81	this work
$[(N4Py)Fe^{III}-O-Mn^{III}(dpaq)]^{3+}$	1.80	2.15		3.56	23
Biological Fe/Mn Species					
RNR1c $Fe^{IV}(\mu\text{-}O)_2Mn^{IV}$	1.81			2.74	12
RNR1c $Fe^{III}(\mu\text{-}O)(\mu\text{-}OH)Mn^{IV}$	Mn−O 1.74			2.91	43
Mt R2lox					
resting state	2.1			3.60	15
$Fe_2^{III}(\mu\text{-}O)$ Complexes					
TPA (no additional bridges)	*1.79*	*2.15*	*2.09*[a], *2.14*[c]	*3.57*	38
$5Et_3TPA^{\dagger}$					
(μ-H_3O_2)	*1.80*	*2.18*	*2.05*[a], *1.91*[b]	*3.35*	38
TPA (μ-H_3O_2)	*1.81*	*2.17*	*2.04*[a], *1.91*[b]	*3.39*	38
BPMEN† (μ-H_3O_2)	*1.82*	*2.23*	*2.05*[a], *1.99*[b]	*3.39*	41
$Fe_2^{III}(\mu\text{-}O)(\mu\text{-}OH)$ Complexes					
TPA*†	*1.88*	*2.15*	*1.93*	*2.79*	25
$6Me_3TPA^{\dagger}$	*1.82*	*2.20*	*1.99*	*2.95*	24
BQPA†	*1.89*	*2.19*	*1.94*	*2.89*	24
BPEEN†	*1.85*	*2.20*	*1.97*	*2.84*	24
$Fe_2^{III}(\mu\text{-}O)_2$ Complexes					
$6Me_3TPA$	1.84 1.92	2.24		2.72	24

[a]Distances indicated in italics are derived from X-ray crystallography, distances in plain text are derived from EXAFS† -TPA* = tris((4-methoxy-3,5-dimethylpyridin-2-yl)methyl)amine; $6Me_3TPA$ = tris((6-methylpyridin-2-yl)methyl)amine; BQPA = 1-(quinolin-2-yl)-*N*,*N*-bis(quinolin-2-ylmethyl)methanamine; BPEEN = *N*,*N*′-diethyl-*N*,*N*′-bis(2-pyridylmethyl)ethane-1,2-diamine; $5Et_3TPA$ = tris((5-ethylpyridin-2-yl)methyl)amine; BPMEN = *N*,*N*′-dimethyl-*N*,*N*′-bis(2-pyridylmethyl)ethane-1,2-diamine; a: it indicates Fe−OH_2 bond length; b: it indicates Fe−OH bond length; and c: it indicates Fe−$OClO_3$ bond length.

data for **1-OH**, **2-OH**, and **3-OH** all show their Mn scatterers with a peak at an $R + \Delta$ value < 3 Å, due to the presence of the Fe(μ-O)(μ-OH)Mn diamond core. Furthermore, the resonance Raman data for **1** and **2** both show closed-core impurities in the presence of water (Figure S8, vide supra). It is probable that the initial preparation of **1** contained excess water, leading to a significant closed-core component. Reanalysis of the 2018 EXAFS data validates this hypothesis (Figure S12 and Tables S2, 1−2018 entries). The data from 2018 is, in fact, best fit with a mixture of Mn scatterers at 3.65 and 2.85 Å, confirming that a mixture was formed in the initial preparation.

The spontaneous formation of closed-core complexes in the presence of water is in direct contrast to what is observed in diferric systems, which bind water to $Fe_2^{III}(\mu\text{-}O)(\mu\text{-}OH)$ cores to form $Fe_2^{III}(\mu\text{-}O)(\mu\text{-}H_3O_2)$ complexes. The aquation equilibria of synthetic Fe/Mn and diferric complexes highlight the differences in the thermodynamic properties that result from incorporating a second metal. The preference for the closed-core confirmation in synthetic systems could shed light on why nature chooses to use heterobimetallic active sites. It is possible that such sites allow for a more diverse array of core structures, or encourage the formation of different core structures, along the oxygen activation pathway.

Based on rR and UV−vis results that show that there is an equilibrium in solution between open- and closed-core compounds, it was of interest to explore the ligand effect on the pK_a of the open-to-closed-core conversion. To this end, each compound was titrated with a variety of bases. Plotting the yield of hydroxo-bridged compounds vs the pK_a of the protonated base generates a sigmoidal plot (Figures 6 and S14−S16). Fitting these data with a Boltzmann function and comparing χ_o values for each compound give the relative acidities of each open-core species. The pK_a values for these compounds are perhaps unexpected (Table 4). Complexes **2** and **3** have essentially the same pK_a (within error), while **1** has

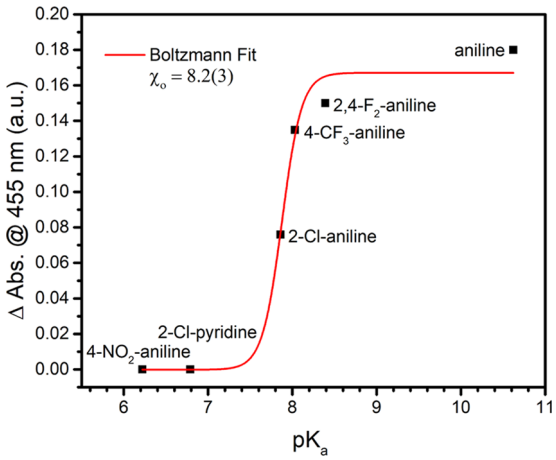

Figure 6. Boltzmann fit of the base-dependent formation of **2-OH** from **2** in MeCN at −40 °C.

https://doi.org/10.1021/acs.inorgchem.1c00684
Inorg. Chem. XXXX, XXX, XXX−XXX

Table 4. pK_a(MeCN) Values for Fe/Mn Compounds

compound	pK_a
1	8.9(1)
2	8.2(3)
3	7.9(1)

a much higher pK_a. One might expect that 5-Me, 3,5-Me, and 4-MeO substitutions on **2** and **3** might decrease the Lewis acidity of these compounds; however, the opposite effect is observed. While the reason for this counterintuitive result is unclear, there must be a strong driving force to form an Fe/Mn diamond core. This is in stark contrast to the diiron counterparts of these compounds, which revert readily to open-core compounds in the presence of water.[24]

To explore differences in reactivity between Fe^{III}/Mn^{III} and diferric complexes, the electron-transfer reactivity of all complexes was assessed with various ferrocenes. Interestingly, **1** and **2** are both able to oxidize diacetyl ferrocene (Figures 7

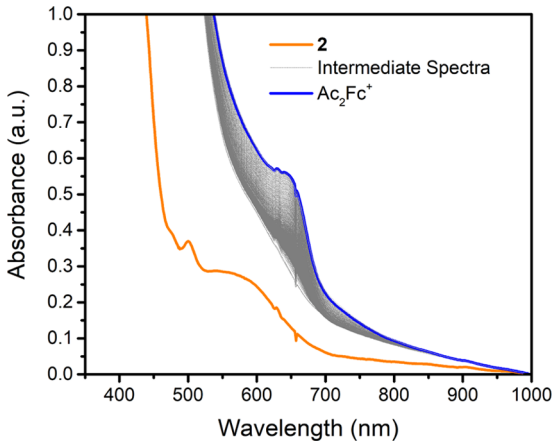

Figure 7. UV−vis spectra of the oxidation of Ac_2Fc by **2** in MeCN at −40 °C.

and S6) (Ac_2Fc, E°(Ac_2Fc^+/Ac_2Fc) = 0.49 V vs Fc^+/Fc),[45] while **3** and the three corresponding $Fe^{III}(\mu\text{-O})(\mu\text{-OH})Mn^{III}$ complexes do not. However, the latter are able to oxidize acetyl ferrocene (Figure S6) (AcFc, E°($AcFc^+/AcFc$) = 0.27 V vs Fc^+/Fc).[45] This behavior is in stark contrast to the diferric $[(L)Fe(OH)(\mu\text{-O})(H_2O)Fe(L)]^{3+}$, complexes (L = TPA, $5Me_3TPA$, and TPA*), none of which are able to oxidize ferrocene (Figure S5). These observations suggest that it is the Mn^{3+} ion that is responsible for oxidizing derivatized ferrocenes.

Recently, Shafaat and co-workers published the protein electrochemistry of R2lox.[26] The cyclic voltammetry of the resting state of wild-type R2lox at pH 7 shows an anodic peak at 0.878 V vs NHE (0.237 V vs Fc^+/Fc) and a cathodic peak at 0.612 V vs NHE (−0.029 V vs Fc^+/Fc). The pH dependence for these electrochemical events shows that the oxidation/reduction is coupled to two proton transfers. While our results do not shed light on proton transfer events, they do show that synthetic compounds are more oxidizing than their protein counterparts by at least 250 mV in the cases of **1** and **2**. The reduction potentials of **3**, **1-OH**, **2-OH**, and **3-OH** are actually comparable to those found for WT R2lox. Based on our results, it also seems likely that electrochemical processes observed in protein arise from the Mn^{3+}/Mn^{2+} couple.

Given the high potentials and known pK_a's of these compounds, the bond dissociation free energy (BDFE) of the O−H bond of water bound to a one-electron reduced $[(L)Fe(OH_2)(\mu\text{-O})Mn(OH_2)(L)]^{4+}$ can be calculated using eq 1, where C is a constant for a given solvent (C_{MeCN} = 52 kcal/mol).[46]

$$\text{BDFE} = 1.37\text{p}K_a + 23.06E^\circ + C \quad (1)$$

Based on eq 1, bond dissociation free energies (BDFEs) for the O−H bond in reduced **1**−**3** can be estimated to be between 68 and 75 kcal/mol. **1-OH**, **2-OH**, and **3-OH** should therefore be able to perform hydrogen atom transfer (HAT) from substrates with X−H BDFE's below 75 kcal/mol (Scheme 2). TEMPO-H (=2,2,6,6-tetramethylpiperidin-1-ol,

Scheme 2. HAT by $Fe^{III}(\mu\text{-O})(\mu\text{-OH})Mn^{III}$ Complexes

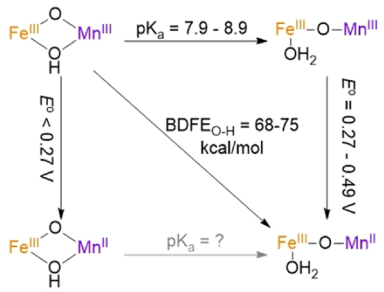

BDFE = 66 kcal/mol)[46] was the substrate of choice to probe this reactivity because of its suitable O−H BDFE. Its high potential (E° = 0.572 V vs Fc/Fc^+)[46] and low acidity (pK_a = 40.1 in MeCN) make it unlikely for a stepwise mechanism to occur. Also, TEMPO-H has been used as a substrate for a wide range of mononuclear Fe^{III}−OH and Mn^{III}−OH compounds, which facilitates comparison between mono- and bimetallic systems.[42,47−49]

The reaction of **1-OH** with TEMPO-H shows a linear dependence on TEMPO-H concentration; the analysis of which gives a second-order rate constant of 0.33 M^{-1} s^{-1} (Figure 8). With TEMPO-D as a substrate, a rate of 0.24 M^{-1} s^{-1} is obtained, corresponding to a kinetic isotope effect of 1.4 that is similar to that found for $[(dpaq)Mn(OH)]^+$ (Table 5). **2-OH** and **3-OH** react with TEMPO-H with a nearly identical rate to **1-OH** (0.32 and 0.37 M^{-1} s^{-1}), respectively, as well as similar KIEs (1.4 vs 1.7 and 2.7) (Table 5 and Figures S17 and S18). These congruent results strongly suggest that all three complexes react with TEMPO-H via the same mechanism. As previously mentioned, the potential and acidity of TEMPO-H make it highly unlikely that a stepwise mechanism (electron transfer−proton transfer or proton transfer−electron transfer) occurs. In fact, hydroxo-bridged compounds are not oxidizing (0.49 V > E° ≥ 0.27 V) nor basic enough (p$K_{a_{1\text{-OH}}}$ = 8.9 p$K_{a_{2\text{-OH}}}$ = 8.2, p$K_{a_{3\text{-OH}}}$ = 7.9) to initiate either electron transfer or proton transfer. For these reasons, we propose that all three complexes oxidize TEMPO-H via hydrogen atom transfer.

When the rates of TEMPO-H oxidation for hydroxo-bridged Fe/Mn compounds are adjusted for temperature differences, they are comparable to that found for $[(TMP)Fe^{III}(OH)]$,[50] but are much slower than the HAT rates for other mononuclear Fe^{III}−OH complexes. The rates of reaction for all three with TEMPO-H are much faster than that for $[(Py5)Fe^{III}(OH)]^{2+}$ with DHA (DHA = 9,10-dihydroanthra-

https://doi.org/10.1021/acs.inorgchem.1c00684
Inorg. Chem. XXXX, XXX, XXX−XXX

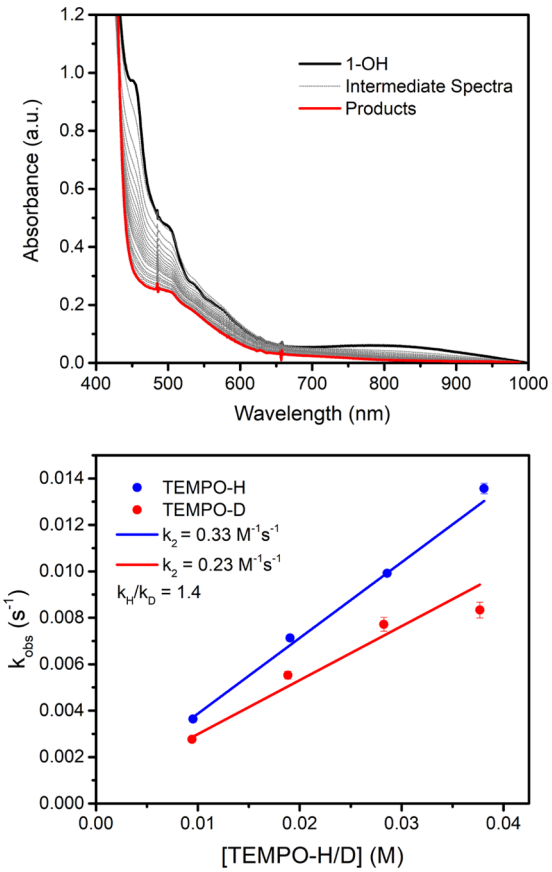

Figure 8. Top: UV−vis spectra for the reaction of 1 mM **1-OH** with 40 mM TEMPOH in MeCN at −40 °C. Bottom: Linear dependence of rate on TEMPO-H/D concentration.

cene), which can be rationalized by the fact the C−H bond in DHA has a C−H BDFE = 76 kcal/mol, which is harder to oxidize than the O−H bond in TEMPO-H with an O−H BDFE = 66 kcal/mol.[46]

The reasons for these differences in reactivity can be explored by comparing the reduction potentials and pK_a's of mononuclear and binuclear complexes. The pK_a's of the Fe^{II}−OH_2 complexes of PY5 and PyPz are both 8, which are comparable to values found for **1-OH** and **2-OH** (although these were measured in DMSO and H_2O at pH 5.2, respectively).[51,52] In the case of the PyPz complex, the Fe^{III}/Fe^{II} potential is 0.477 V vs Fc^+/Fc, significantly more oxidizing than heterobimetallic complexes. Surprisingly, the redox potential of the PY5 complex is lower than those for **1-OH**, **2-OH**, and **3-OH** (0.155 V vs Fc^+/Fc);[52] so the reason for the difference in observed reactivity is not as straightforward to rationalize, although the differences in the substrate and solvent conditions make any comparison imperfect.

The HAT reactivity of bimetallic complexes appears to be more similar to that of mononuclear Mn^{III}−OH complexes than for Fe^{III}−OH complexes. Indeed the rates of reaction with TEMPO-H for the series of $[(dpaq)Mn(OH)]^+$ complexes are all within 1 order of magnitude of the rates of **1-OH**, **2-OH**, and **3-OH**. Furthermore, the H/D KIE for the reaction of $[(dpaq)Mn(OH)]^+$ is nearly identical to that of **2-OH**. These similarities suggest that the Mn^{III} ion likely exerts a greater influence over the reactivity of Fe/Mn complexes than the Fe^{III} ion.

In examining the thermodynamics that drives HAT by Mn^{III}−OH compounds, the data show that the reduction potentials of dpaq complexes, which range from −0.72 to −0.57 V vs Fc^+/Fc, are all much lower than what is found for the Fe/Mn complexes reported here.[48] Similarly, the reduction potential of $[(S^{Me2}N_4(tren))Mn(OH)]^+$ (−0.241 V vs Fc^+/Fc) is much lower than those of Fe/Mn compounds. These lower reduction potentials are perhaps not unexpected given the anionic ligands used to support these Mn^{III}−OH complexes. The lower reduction potentials, however, are compensated for by a much higher basicity in the case of dpaq compounds, with Mn^{II}−OH_2 pK_a's that range from 27.8 to 29.5.[48] $[(S^{Me2}N_4(tren))Mn(OH)]^+$ has a much lower pK_a than Fe/Mn complexes (pK_a = 5.3). This would suggest that $[(S^{Me2}N_4(tren))Mn(OH)]^+$ would be the less competent oxidant. However, even when adjusted for temperature, it is still an order of magnitude faster than **1-OH** and **2-OH** at HAT. However, the HAT reactivity of $[(S^{Me2}N_4(tren))Mn(OH)]^+$ was probed in water, which makes it an imperfect comparison.

Another possible reason for differences in observed HAT reactivity between the newly reported heterobimetallic compounds and the mononuclear complexes is the nature of the hydroxo moiety. In the case of mononuclear compounds,

Table 5. Comparison of Substrate Oxidation Rates for Fe^{III}−OH and Mn^{III}−OH Complexes[b]

complex	substrate	T (°C)	k_2	H/D KIE	refs
1-OH	TEMPOH	−40	0.33	1.4	[a]
2-OH	TEMPOH	−40	0.32	1.7	[a]
3-OH	TEMPOH	−40	0.37	2.7	[a]
$[(TMC\text{-}py)Fe(OH)]^{2+}$	TEMPOH	−40	7.1	6	42
(TMP)Fe(OH)	TEMPOH	25	76		50
$[(PyPz)Fe(OH_2)(OH)]^{4+}$	xanthene	20	2.2×10^3	20	51
$[(Py5)Fe(OH)]^{2+}$	DHA	25	4.3×10^{-4}	6.3	52
$[(dpaq)Mn(OH)]^+$	TEMPOH	25	0.13	1.8	53
$[(dpaq^{2Me})Mn(OH)]^+$	TEMPOH	−35	3.9	2.7	47
$[(dpaq^{5Cl})Mn(OH)]^+$	TEMPOH	−35	2.8		48
$[(dpaq^{5NO2})Mn(OH)]^+$	TEMPOH	−35	7		48
$[(S^{Me2}N_4(tren))\text{-}Mn(OH)]^+$	TEMPOH	25	2.1×10^3	3.1	49

[a]This work. [b]Abbreviations used: TMC-py = 1-(pyridyl-2′-methyl)-4,8,11-trimethyl-1,4,8,11-tetrazacyclotetradecane, Py5 = 2,6-bis(bis(2-pyridyl)methoxymethane)pyridine, TMP = meso-tetramesitylporphyrinate; PyPz = quaternized tetra-2,3-pyridinoporphyrazine, and dpaq = 2-(bis(pyridin-2-ylmethyl)amino)-*N*-(quinolin-8-yl)acetamidate anion.

https://doi.org/10.1021/acs.inorgchem.1c00684
Inorg. Chem. XXXX, XXX, XXX−XXX

hydroxide is terminal, while hydroxide acts as a bridge in Fe/Mn compounds. In high-valent diiron chemistry, the switch from a bridging oxo moiety to a terminal oxo unit can result in as much as a million-fold increase in HAT reactivity.[54] While differences between mononuclear Mn^{III}−OH and Fe^{III}−OH complexes and Fe/Mn complexes are not quite as stark, it could still be a key structural feature that leads to enhanced HAT rates for mononuclear complexes.

■ CONCLUSIONS

This work demonstrates the synthesis of a novel series of Fe/Mn compounds. Importantly, these compounds serve as the first to model the diamond core structures of proposed intermediates along the oxygen activation pathway of RNR 1c and R2lox. The first synthetic complexes with Fe/Mn diamond cores have thus been characterized, and their spontaneous formation from their linear Fe^{III}−O−Mn^{III} precursors in the presence of excess water has been documented. In contrast to the diiron chemistry, Fe/Mn compounds prefer to form closed-core compounds in the presence of water, an unexpected result. Furthermore, the electron-transfer reactivity of Fe/Mn compounds was compared to their diiron counterparts. In all cases, Fe/Mn compounds are more oxidizing than their diiron counterparts—especially in the case of **1** and **2**, which are at least 490 mV more oxidizing than their diiron counterparts. Taken together, these results suggest that Nature uses heterobimetallic active sites to control the preference for diamond core intermediates and to modulate the reduction potential of oxidative intermediates in key enzymatic reactions.

The series of synthetic Fe/Mn compounds exhibit an unexpected relationship between the basicity of the iron supporting ligand and the pK_a of the conversion from open core to closed core. While reasons for this inverse relationship are unclear, it nonetheless illustrates differences between diiron and Fe/Mn chemistry.

Using the electrochemical and pK_a data, we were able to estimate the BDFE of water bound to the reduced form of Fe/Mn compounds. This estimation led us to attempt HAT reactivity with TEMPO-H. All three complexes react with TEMPO-H via an HAT mechanism. The rates of these reactions are comparable to those for mononuclear Fe^{III}−OH and Mn^{III}−OH compounds for X−H (X = C, O) bond activation chemistry and serve as the first examples of Fe/Mn complexes that perform HAT reactions.

Five new Fe/Mn compounds have been characterized using a variety of spectroscopic techniques. Three of these compounds are the first examples of synthetic Fe/Mn diamond cores. While it should be noted that none of these compounds model the high-valent oxidation states of the proposed enzymatic intermediates, they still serve as structural and spectroscopic mimics of RNR 1c and R2lox—the first of their kind.

■ EXPERIMENTAL SECTION

Commercially available chemicals such as all bases used, perchloric acid, etc., were purchased from commercial sources and used without further purification unless otherwise noted. TEMPO-H was prepared according to the literature procedure[55] and TEMPO-D was prepared following an analogous procedure using deuterated solvents. $Mn^{II}(TPA)(OTf)_2$ and $[Fe(TPA)(MeCN)_2](OTf)_2$ were prepared according to literature procedures.[56,57] The corresponding $Fe^{II}(5Me_3TPA)$ and $Fe^{II}(TPA^*)$ complexes were prepared using analogous procedures. 1-(*tert*-Butylsulfonyl)-2-iodosylbenzene was prepared according to a literature procedure.[58]

Low-temperature UV−visible absorption spectra were recorded on an HP 8453A diode array spectrometer fitted with a cryostat obtained from UNISOKU Scientific Instruments, Japan. Raman spectra were collected with an Acton AM-506 monochromator equipped with a Princeton LN/CCD data collection system, with excitation by 405/457/515/561 nm solid-state lasers from Cobolt Lasers, Inc. Spectra in acetonitrile were collected at 77 K using a 135° backscattering geometry and at 233 K using a 90° backscattering geometry. The detector was cooled to −120 °C prior to the experiments. Spectral calibration was performed on a 1:1 v/v mixture of acetonitrile and toluene. The collected data were processed using Spectragryph.[59] A multipoint baseline correction was performed for all spectra. X-band EPR spectra were collected at 30 K on a Bruker Elexsys E-500 spectrometer equipped with an Oxford ESR-910 cryostat. EPR integrations were carried out using EasySpin (version 5.2.25) in the Simultispin GUI.[60,61] The area under the double integral of an aqueous 1.35 mM $Cu(ClO4)_2$ solution was compared to the area under the double integral of Fe/Mn complexes. This ratio was then used to establish the concentration of heterobimetallic complexes in the solution. EPR simulations were carried out using SpinCount software developed by Prof. Michael Hendrich at Carnegie Mellon University.[62] Iron K-edge X-ray absorption spectra were collected on SSRL beamline 9−3 using a 100-element solid-state Ge detector (Canberra) with a SPEAR storage ring current of ∼500 mA at a power of 3.0 GeV. The incoming X-rays were unfocused using a Si(220) double-crystal monochromator, which was detuned to 70% of the maximal flux to attenuate harmonic X-rays. Between six and eight scans of the fluorescence excitation spectra for each sample were collected from 6882 to 8000 eV at a temperature (10 K) that was controlled by an Oxford Instruments CF1208 continuous-flow liquid helium cryostat. An iron foil was placed in the beam pathway prior to the ionization chamber (Io) and scanned concomitantly for energy calibration, with the first inflection point of the edge assigned to 7112.0 eV. A 3, 6, or 9 μm Mn filter and a Soller slit were used to increase the signal-to-noise ratio of the spectra. Photoreduction was monitored by scanning the same spot on the sample twice and comparing the first-derivative peaks associated with the edge energy during collection, but none was observed in the present study. The detector channels from the scans were examined, calibrated, averaged, and processed for EXAFS analysis using EXAFSPAK to extract $\chi(k)$. Theoretical phase and amplitude parameters for a given absorber−scatterer pair were calculated using FEFF 8.40 and were utilized by the "opt" program of the EXAFSPAK package during curve fitting. In all analyses, the coordination number of a given shell was a fixed parameter and was varied iteratively in integer steps, while bond lengths (R) and mean-square deviation ($\sigma 2$) were allowed to float freely. The amplitude reduction factor S0 was fixed at 0.9, while the edge-shift parameter E0 was allowed to float as a single value for all shells. Thus, in any given fit, the number of floating parameters was typically equal to (2 × number of shells) + 1. The k range of the data is 2−15 $Å^{-1}$. Pre-edge analysis was performed on data normalized in the "process" program of the EXAFSPAK package, and pre-edge features were fit between 7108 and 7118 eV using the Fityk program with pseudo-Voigt functions composed of 50:50 Gaussian/Lorentzian functions.[40,63]

Sample Preparation Procedures. EPR and rR samples were prepared in a similar manner. In air, a 1 mM solution of the Fe(II) precursor was cooled to −40 °C in the UV−vis cryostat. To this solution was added 1 equiv of 1-(*tert*-butylsulfonyl)-2-iodosylbenzene to generate the corresponding Fe(IV)O complex. To the Fe(IV) compound was added 1 equiv of $(TPA)Mn(OTf)_2$. In the case of **1**, **2**, and **3**, the reaction was monitored until the Fe/Mn compound was maximally formed, then transferred with a precooled pipette to an EPR tube and frozen in a liquid nitrogen bath. This procedure differed for rR spectra collected at 233 K. These samples were transferred to flat-bottom NMR tubes and transferred to a −40 °C bath before spectra were collected. **1-OH**, **2-OH**, and **3-OH** were generated from

https://doi.org/10.1021/acs.inorgchem.1c00684
Inorg. Chem. XXXX, XXX, XXX−XXX

solutions of **1**, **2**, and **3** by the addition of 1 equiv of triethylamine. These samples were frozen in a similar manner to **1**, **2**, and **3**.

EXAFS samples were prepared by analogous methods to the EPR and rR samples, but from 5 mM Fe(II) solutions. These solutions of Fe/Mn complexes were transferred to Mössbauer cups and frozen in liquid N2.

pK_a Determination. The pK_a of each complex was determined using the following procedures. A 1 mM, 1.2 mL of MeCN solution of the starting Fe^{II} complex was cooled to −40 °C in the UV−vis cryostat. To this, 12 μL of 0.1 M sArIO (1 equiv) dissolved in 2,2,2-trifluoroethanol was added to generate the Fe^{IV}═O complex. Then, 12 μL of 0.1 M $Mn^{II}(TPA)(OTf)_2$ was added in MeCN (1 equiv). Once the $Fe^{III}(\mu\text{-O})Mn^{III}$ complex had been fully formed, 12 μL of 0.1 M solution of a given base was added to the solution. The change in absorbance at 455 nm was noted. This was repeated in triplicate for each base. A plot of the change in absorbance at 455 nm with respect to the pK_a of the conjugate acid of the titrated base was generated for each trial. This was then fit using a sigmoidal Boltzmann function with a Levenberg Marquardt iteration algorithm in Origin 2016. The χ_o values generated from these fits were then averaged across the three trials for each compound.

Electron-Transfer Experiments. A 1 mM, 1.2 mL of MeCN solution of the starting Fe^{II} complex was cooled to −40 °C in the UV−vis cryostat. To this, was added 12 μL of 0.1 M sArIO (1 equiv) dissolved in 2,2,2-trifluoroethanol to generate the Fe^{IV}═O complex. Then, in the solution, was added 12 μL of 0.1 M $Mn^{II}(TPA)(OTf)_2$ in MeCN (1 equiv). Once the $Fe^{III}(\mu\text{-O})Mn^{III}$ complex had been fully formed, 12 μL of either Ac_2Fc or AcFc was added to the open-core complex and the reaction was monitored for the formation of the corresponding ferrocenium cation. In the case of the (μ-O)(μ-OH) complexes, 12 μL of 0.1 M TEA in MeCN were added first. Once the (μ-O)(μ-OH) complexes were formed in full yield, 12 μL of 0.1 M AcFc were added to the solution and the reaction was monitored for the formation of the corresponding ferrocenium cation.

Kinetics Experiments. All kinetics measurements were performed using analogous procedures. A 1 mM, 1.2 mL of MeCN solution of the starting Fe^{II} complex was cooled to −40 °C in the UV−vis cryostat. To this, was added 12 μL of 0.1 M sArIO (1 equiv) dissolved in 2,2,2-trifluoroethanol to generate the Fe^{IV}═O complex. Then, in the solution, was added 12 μL of 0.1 M $Mn^{II}(TPA)(OTf)_2$ in MeCN (1 equiv). Once the $Fe^{III}(\mu\text{-O})Mn^{III}$ complex had been fully formed, 12 μL of 0.1 M 2,4,6-trimethyl-pyridine was added (1 equiv) to form the corresponding $Fe^{III}(\mu\text{-O})(\mu\text{-OH})Mn^{III}$ complex. To this solution, was added 24 μL of either 0.5 M (10 equiv), 1 M (20 equiv), 1.5 M (30 equiv), or 2 M (40 equiv) of TEMPO-H or TEMPO-D. The change in absorption of the 455 nm peak was monitored over time. Three trials of each concentration were performed, and the decay of the 455 nm peak was fit with a single exponential. The k_{obs} for each concentration was averaged over the three trials and plotted with respect to the substrate concentration to give a second-order rate constant plot.

■ ASSOCIATED CONTENT

Supporting Information

The Supporting Information is available free of charge at https://pubs.acs.org/doi/10.1021/acs.inorgchem.1c00684.

UV−vis, resonance Raman, and XAS spectra; EXAFS fitting tables; pK_a determinations; and kinetic analyses (PDF)

■ AUTHOR INFORMATION

Corresponding Author

Yisong Guo − *Department of Chemistry, Carnegie Mellon University, Pittsburgh, Pennsylvania 15213, United States;* orcid.org/0000-0002-4132-3565; Email: larryque@umn.edu

Author

Patrick M. Crossland − *Department of Chemistry and Center for Metals in Biocatalysis, University of Minnesota, Minneapolis, Minnesota 55455, United States;* orcid.org/0000-0001-7819-371X

Complete contact information is available at: https://pubs.acs.org/10.1021/acs.inorgchem.1c00684

Notes

The authors declare no competing financial interest.

■ ACKNOWLEDGMENTS

Efforts at the University of Minnesota are supported by the National Institutes of Health (R35 GM-131721), while those at Carnegie Mellon University are supported by the National Science Foundation (CHE-1654060). XAS experiments were performed at Stanford Synchrotron Radiation Lightsource (SSRL). Use of the Stanford Synchrotron Radiation Lightsource, SLAC National Accelerator Laboratory, is supported by the U.S. Department of Energy, Office of Science, Office of Basic Energy Sciences under Contract No. DE-AC02-76SF00515. The SSRL Structural Molecular Biology Program is supported by the DOE Office of Biological and Environmental Research, and by the National Institutes of Health, National Institute of General Medical Sciences (P30GM133894). The contents of this publication are solely the responsibility of the authors and do not necessarily represent the official views of NIGMS or NIH.

■ REFERENCES

(1) Costas, M.; Mehn, M. P.; Jensen, M. P.; Que, L. Dioxygen Activation at Mononuclear Nonheme Iron Active Sites: Enzymes, Models, and Intermediates. *Chem. Rev.* **2004**, *104*, 939−986.

(2) Jasniewski, A. J.; Que, L. Dioxygen Activation by Nonheme Diiron Enzymes: Diverse Dioxygen Adducts, High-Valent Intermediates, and Related Model Complexes. *Chem. Rev.* **2018**, *118*, 2554−2592.

(3) Solomon, E. I.; Heppner, D. E.; Johnston, E. M.; Ginsbach, J. W.; Cirera, J.; Qayyum, M.; Kieber-Emmons, M. T.; Kjaergaard, C. H.; Hadt, R. G.; Tian, L. Copper Active Sites in Biology. *Chem. Rev.* **2014**, *114*, 3659−3853.

(4) McEvoy, J. P.; Brudvig, G. W. Water-Splitting Chemistry of Photosystem II. *Chem. Rev.* **2006**, *106*, 4455−4483.

(5) Yoshikawa, S.; Shimada, A. Reaction Mechanism of Cytochrome c Oxidase. *Chem. Rev.* **2015**, *115*, 1936−1989.

(6) Jiang, W.; Yun, D.; Saleh, L.; Barr, E.; Xing, G.; Hoffart, L. M.; Maslak, M.; Krebs, C.; Bollinger, J. M., Jr. A Manganese (IV)/Iron (III) Cofactor in *Chlamydia Trachomatis* Ribonucleotide Reductase. *Science* **2007**, *316*, 1188−1191.

(7) Schmidt, F.; Donahoe, S.; Hagens, K.; Mattow, J.; Schaible, U. E.; Kaufmann, S. H. E.; Aebersold, R.; Jungblut, P. R. Complementary Analysis of the *Mycobacterium tuberculosis* Proteome by Two-Dimensional Electrophoresis and Isotope-Coded Affinity Tag Technology. *Mol. Cell. Proteomics* **2004**, *3*, 24−42.

(8) Jiang, W.; Yun, D.; Saleh, L.; Bollinger, J. M.; Krebs, C. Formation and Function of the Manganese (IV)/ Iron (III) Cofactor in *Chlamydia trachomatis* Ribonucleotide Reductase. *Biochemistry* **2008**, *47*, 13736−13744.

(9) Dassama, L. M. K.; Jiang, W.; Varana, P. T.; Pandelia, M.-E.; Conner, D. A.; Xie, J.; Bollinger, J. M.; Krebs, C. Radical-Translocation Intermediates and Hurdling of Pathway Defects in "Super-Oxidized" (Mn(IV)/Fe(IV)) *Chlamydia trachomatis* Ribonucleotide Reductase. *J. Am. Chem. Soc.* **2012**, *134*, 20498−20506.

(10) Miller, E. K.; Trivelas, N. E.; Maugeri, P. T.; Blaesi, E. J.; Shafaat, H. S. Time-Resolved Investigations of Heterobimetallic

Cofactor Assembly in R2lox Reveal Distinct Mn/Fe Intermediates. *Biochemistry* **2017**, *56*, 3369−3379.

(11) Jiang, W.; Hoffart, L. M.; Krebs, C.; Bollinger, J. M. A Manganese (IV)/ Iron (IV) Intermediate in Assembly of the Manganese (IV)/ Iron (III) Cofactor of *Chlamydia trachomatis* Ribonucleotide Reductase. *Biochemistry* **2007**, *46*, 8709−8716.

(12) Martinie, R. J.; Blaesi, E. J.; Krebs, C.; Martin Bollinger, J.; Silakov, A.; Pollock, C. J. Evidence for a Di-μ-Oxo Diamond Core in the Mn(IV)/Fe(IV) Activation Intermediate of Ribonucleotide Reductase from *Chlamydia trachomatis*. *J. Am. Chem. Soc.* **2017**, *139*, 1950−1957.

(13) Bollinger, J. M.; Jiang, W.; Green, M. T.; Krebs, C. The Manganese(IV)/Iron(III) Cofactor of *Chlamydia trachomatis* Ribonucleotide Reductase: Structure, Assembly, Radical Initiation, and Evolution. *Curr. Opin. Struct. Biol.* **2008**, *18*, 650−657.

(14) Dassama, L. M. K.; Krebs, C.; Bollinger, J. M.; Rosenzweig, A. C.; Boal, A. K. Structural Basis for Assembly of the Mn(IV)/Fe(III) Cofactor in the Class 1c Ribonucleotide Reductase from *Chlamydia trachomatis*. *Biochemistry* **2013**, *52*, 6424−6436.

(15) Andersson, C. S.; Högbom, M. A Mycobacterium Tuberculosis Ligand-Binding Mn/Fe Protein Reveals a New Cofactor in a Remodeled R2-Protein Scaffold. *Proc. Natl. Acad. Sci. U.S.A.* **2009**, *106*, 5633−5638.

(16) McDonald, A. R.; Que, L. High-Valent Nonheme Iron-Oxo Complexes: Synthesis, Structure, and Spectroscopy. *Coord. Chem. Rev.* **2013**, *257*, 414−428.

(17) Paul, S.; Neese, F.; Pantazis, D. A. Structural Models of the Biological Oxygen-Evolving Complex: Achievements, Insights, and Challenges for Biomimicry. *Green Chem.* **2017**, *19*, 2309.

(18) Elwell, C. E.; Gagnon, N. L.; Neisen, B. D.; Dhar, D.; Spaeth, A. D.; Yee, G. M.; Tolman, W. B. Copper-Oxygen Complexes Revisited: Structures, Spectroscopy, and Reactivity. *Chem. Rev.* **2017**, *117*, 2059−2107.

(19) Hotzelmann, R.; Wieghardt, K.; Flörke, U.; Haupt, H. J.; Weatherburn, D. C.; Bonvoisin, J.; Blondin, G.; Girerd, J. J. Spin Exchange Coupling in Asymmetric Heterodinuclear Complexes Containing the μ-Oxo-Bis(μ-Acetato)Dimetal Core. *J. Am. Chem. Soc.* **1992**, *114*, 1681−1696.

(20) Holman, T. R.; Wang, Z.; Hendrich, M. P.; Que, L. Structural and Spectroscopic Properties of Antiferromagnetically Coupled FeIIIMnII and FeIIMnII Complexes. *Inorg. Chem.* **1995**, *34*, 134−139.

(21) Carboni, M.; Clémancey, M.; Molton, F.; Pécaut, J.; Lebrun, C.; Dubois, L.; Blondin, G.; Latour, J. M. Biologically Relevant Heterodinuclear Iron-Manganese Complexes. *Inorg. Chem.* **2012**, *51*, 10447−10460.

(22) Das, B.; Daver, H.; Singh, A.; Singh, R.; Haukka, M.; Demeshko, S.; Meyer, F.; Lisensky, G.; Jarenmark, M.; Himo, F.; et al. A Heterobimetallic FeIIIMnII Complex of an Unsymmetrical Dinucleating Ligand: A Structural and Functional Model Complex for the Active Site of Purple Acid Phosphatase of Sweet Potato. *Eur. J. Inorg. Chem.* **2014**, *2014*, 2204−2212.

(23) Zhou, A.; Crossland, P. M.; Draksharapu, A.; Jasniewski, A. J.; Kleespies, S. T.; Que, L. Oxoiron(IV) Complexes as Synthons for the Assembly of Heterobimetallic Centers Such as the Fe/Mn Active Site of Class Ic Ribonucleotide Reductases. *JBIC, J. Biol. Inorg. Chem.* **2018**, *23*, 155−165.

(24) Zheng, H.; Zang, Y.; Dong, Y.; Young, V. G.; Que, L. Complexes with $Fe(III)_2(\mu\text{-}O)(\mu\text{-}OH)$, $Fe(III)_2(\mu\text{-}O)_2$, and $[Fe(III)_3(M_2\text{-}O)_3]$ Cores: Structures, Spectroscopy, and Core Interconversions. *J. Am. Chem. Soc.* **1999**, *121*, 2226−2235.

(25) Do, L. H.; Xue, G.; Que, L.; Lippard, S. J. Evaluating the Identity and Diiron Core Transformations of a (μ-Oxo)Diiron(III)-Complex Supported by Electron-Rich Tris(Pyridyl-2-Methyl) Amine Ligands. *Inorg. Chem.* **2012**, *51*, 2393−2402.

(26) Shafaat, H. S.; Kisgeropoulos, E. C.; Griese, J. J.; Smith, Z. R.; Branca, R. M. M.; Schneider, C. R.; Högbom, M. Key Structural Motifs Balance Metal Binding and Oxidative Reactivity in a Heterobimetallic Mn/Fe Protein. *J. Am. Chem. Soc.* **2020**, *142*, 5338−5354.

(27) Duboc, C. Determination and Prediction of the Magnetic Anisotropy of Mn Ions. *Chem. Soc. Rev.* **2016**, *45*, 5834−5847.

(28) Gupta, R.; Lacy, D. C.; Bominaar, E. L.; Borovik, A. S.; Hendrich, M. P. Electron Paramagnetic Resonance and Mössbauer Spectroscopy and Density Functional Theory Analysis of a High-Spin Fe IV-Oxo Complex. *J. Am. Chem. Soc.* **2012**, *134*, 9775−9784.

(29) Bigi, J. P.; Harman, W. H.; Lassalle-Kaiser, B.; Robles, D. M.; Stich, T. A.; Yano, J.; Britt, R. D.; Chang, C. J. A High-Spin Iron(IV)-Oxo Complex Supported by a Trigonal Nonheme Pyrrolide Platform. *J. Am. Chem. Soc.* **2012**, *134*, 1536−1542.

(30) Sanders-Loehr, J.; Wheeler, W. D.; Shiemke, A. K.; Averill, B. A.; Loehr, T. M. Electronic and Raman Spectroscopic Properties of Oxo-Bridged Dinuclear Iron Centers in Proteins and Model Compounds. *J. Am. Chem. Soc.* **1989**, *111*, 8084−8093.

(31) Shiemke, A. K.; Loehr, T. M.; Sanders-Loehr, J. Resonance Raman Study of the μ-Oxo-Bridged Binuclear Iron Center in Oxyhemerythrin. *J. Am. Chem. Soc.* **1984**, *106*, 4951−4956.

(32) Norman, R. E.; Yan, S.; Que, L.; Backes, G.; Ling, J.; Sanders-Loehr, J.; Zhang, J. H.; O'Connor, C. J. (μ-Oxo)(μ-Carboxylato)-Diiron(III) Complexes with Distinct Iron Sites. Consequences of the Inequivalence and Its Relevance to Dinuclear Iron-Oxo Proteins. *J. Am. Chem. Soc.* **1990**, *112*, 1554−1562.

(33) Wilkinson, E. C.; Dong, Y.; Zang, Y.; Fujii, H.; Faczkiewicz, R.; Faczkiewicz, G.; Czernuszewicz, R. S.; Que, L., Jr. Raman Signature of the Fe_2O_2 "diamond" Core. *J. Am. Chem. Soc.* **1998**, *120*, 955−962.

(34) Hsu, H. F.; Dong, Y.; Shu, L.; Young, V. G.; Que, L. Crystal Structure of a Synthetic High-Valent Complex with an $Fe_2(\mu\text{-}O)_2$ Diamond Core. Implications for the Core Structures of Methane Monooxygenase Intermediate Q and Ribonucleotide Reductase Intermediate X. *J. Am. Chem. Soc.* **1999**, *121*, 5230−5237.

(35) Skulan, A. J.; Hanson, M. A.; Hsu, H. F.; Que, L.; Solomon, E. I. Spectroscopic Study of $[Fe_2O_2(5\text{-}Et_3\text{-}TPA)_2]3+$: Nature of the Fe_2O_2 Diamond Core and Its Possible Relevance to High-Valent Binuclear Non-Heme Enzyme Intermediates. *J. Am. Chem. Soc.* **2003**, *125*, 7344−7356.

(36) Xue, G.; Wang, D.; De Hont, R.; Fiedler, A. T.; Shan, X.; Münck, E.; Que, L. A Synthetic Precedent for the [FeIV2(μ-O) 2] Diamond Core Proposed for Methane Monooxygenase Intermediate Q. *Proc. Natl. Acad. Sci. U.S.A.* **2007**, *104*, 20713−20718.

(37) Banerjee, S.; Draksharapu, A.; Crossland, P. M.; Fan, R.; Guo, Y.; Swart, M.; Que, L. Sc3+-Promoted O−O Bond Cleavage of a (μ-1,2-Peroxo)Diiron(III) Species Formed from an Iron(II) Precursor and O2 to Generate a Complex with an FeIV2(μ-O)2Core. *J. Am. Chem. Soc.* **2020**, *142*, 4285−4297.

(38) Dong, Y.; Fujii, H.; Hendrich, M. P.; Leising, R. A.; Pan, G.; Randall, C. R.; Wilkinson, E. C.; Zang, Y.; Que, L.; Fox, B. G.; et al. A High-Valent Nonheme Iron Intermediate. Structure and Properties of $[Fe_2(\mu\text{-}O)_2(5\text{-}Me\text{-}TPA)_2]$ $(ClO_4)_3$. *J. Am. Chem. Soc.* **1995**, *117*, 2778−2792.

(39) Que, L., Jr.; Tolman, W. B. Bis(μ-Oxo)Dimetal "Diamond" Cores in Copper and Iron Complexes Relevant to Biocatalysis. *Angew. Chem., Int. Ed.* **2002**, *41*, 1114−1137.

(40) Westre, T. E.; Kennepohl, P.; Dewitt, J. G.; Hedman, B.; Hodgson, K. O.; Solomon, E. I.; V, S. U. A Multiplet Analysis of Fe K-Edge 1s f 3d Pre-Edge Features of Iron Complexes. *J. Am. Chem. Soc.* **1997**, *119*, 6297−6314.

(41) Poussereau, S.; Blondin, G.; Cesario, M.; Guilhem, J.; Chottard, G.; Gonnet, F.; Girerd, J. J. Synthesis, Structure, and Characterization of the New [L(OH)Fe(μ-O)Fe(OH2)L]3+ Complex (L = N,N'-Dimethyl-N,N'-Bis(2-Pyridylmethyl)Ethane-1,2-Diamine). Detection of an Equilibrium with the Protonated Diamond Form [LFe(μ-O)(μ-OH)FeL]3+ in Acetonitrile. *Inorg. Chem.* **1998**, *37*, 3127−3132.

(42) Ching, W.; Zhou, A.; Klein, J. E. M. N.; Fan, R.; Knizia, G.; Cramer, C. J.; Guo, Y.; Que, L. Characterization of the Fleeting Hydroxoiron (III) Complex of the Pentadentate TMC-Py Ligand. *Inorg. Chem.* **2017**, *56*, 11129−11140.

https://doi.org/10.1021/acs.inorgchem.1c00684
Inorg. Chem. XXXX, XXX, XXX−XXX

(43) Younker, J. M.; Krest, C. M.; Jiang, W.; Krebs, C.; Bollinger, J. M.; Green, M. T. Structural Analysis of the Mn (IV)/ Fe (III) Cofactor of *Chlamydia trachomatis* Ribonucleotide Reductase by Extended X-Ray Absorption Fine Structure Spectroscopy and Density Functional Theory Calculations. *J. Am. Chem. Soc.* **2008**, *130*, 15022−15027.

(44) Dong, Y.; Zang, Y.; Shu, L.; Wilkinson, E. C.; Que, L.; Kauffmann, K.; Münck, E. Models for Nonheme Diiron Enzymes. Assembly of a High-Valent Fe2(μ-O)2 Diamond Core from Its Peroxo Precursor. *J. Am. Chem. Soc.* **1997**, *119*, 12683−12684.

(45) Connelly, N. G.; Geiger, W. E. Chemical Redox Agents for Organometallic Chemistry. *Chem. Rev.* **1996**, *96*, 877−910.

(46) Wise, C. F.; Agarwal, R. G.; Mayer, J. M. Determining Proton-Coupled Standard Potentials and X-H Bond Dissociation Free Energies in Nonaqueous Solvents Using Open-Circuit Potential Measurements. *J. Am. Chem. Soc.* **2020**, *142*, 10681−10691.

(47) Rice, D. B.; Wijeratne, G. B.; Burr, A. D.; Parham, J. D.; Day, V. W.; Jackson, T. A. Steric and Electronic Influence on Proton-Coupled Electron-Transfer Reactivity of a Mononuclear Mn(III)-Hydroxo Complex. *Inorg. Chem.* **2016**, *55*, 8110−8120.

(48) Rice, D. B.; Munasinghe, A.; Grotemeyer, E. N.; Burr, A. D.; Day, V. W.; Jackson, T. A. Structure and Reactivity of (μ-Oxo)Dimanganese(III,III) and Mononuclear Hydroxomanganese-(III) Adducts Supported by Derivatives of an Amide-Containing Pentadentate Ligand. *Inorg. Chem.* **2019**, *58*, 622−636.

(49) Coggins, M. K.; Brines, L. M.; Kovacs, J. A. Synthesis and Structural Characterization of a Series of MnIIIOR Complexes, Including a Water-Soluble MnIIIOH That Promotes Aerobic Hydrogen-Atom Transfer. *Inorg. Chem.* **2013**, *52*, 12383−12393.

(50) Porter, T. R.; Mayer, J. M. Radical Reactivity of the Fe(III)/(II) Tetramesitylporphyrin Couple: Hydrogen Atom Transfer, Oxyl Radical Dissociation, and Catalytic Disproportionation of a Hydroxylamine. *Chem. Sci.* **2014**, *5*, 372−380.

(51) Gao, H.; Groves, J. T. Fast Hydrogen Atom Abstraction by a Hydroxo Iron(III) Porphyrazine. *J. Am. Chem. Soc.* **2017**, *139*, 3938−3941.

(52) Goldsmith, C. R.; Stack, T. D. P. Hydrogen Atom Abstraction by a Mononuclear Ferric Hydroxide Complex: Insights into the Reactivity of Lipoxygenase. *Inorg. Chem.* **2006**, *45*, 6048−6055.

(53) Wijeratne, G. B.; Corzine, B.; Day, V. W.; Jackson, T. A. Saturation Kinetics in Phenolic O−H Bond Oxidation by a Mononuclear Mn(III)−OH Complex Derived from Dioxygen. *Inorg. Chem.* **2014**, *53*, 7622−7634.

(54) Xue, G.; De Hont, R.; Münck, E.; Que, L. Million-Fold Activation of the [Fe2 (μ-O)2] Diamond Core for C-H Bond Cleavage. *Nat. Chem.* **2010**, *2*, 400−405.

(55) Mader, E. A.; Larsen, A. S.; Mayer, J. M. Hydrogen Atom Transfer from Iron(II)-Tris[2,2′- Bi(Tetrahydropyrimidine)] to TEMPO: A Negative Enthalpy of Activation Predicted by the Marcus Equation. *J. Am. Chem. Soc.* **2004**, *126*, 8066−8067.

(56) Lim, M. H.; Rohde, J. U.; Stubna, A.; Bukowski, M. R.; Costas, M.; Ho, R. Y. N.; Münck, E.; Nam, W.; Que, L. An FeIV=O Complex of a Tetradentate Tripodal Nonheme Ligand. *Proc. Natl. Acad. Sci. U.S.A.* **2003**, *100*, 3665−3670.

(57) Ward, A. L.; Elbaz, L.; Kerr, J. B.; Arnold, J. Nonprecious Metal Catalysts for Fuel Cell Applications: Electrochemical Dioxygen Activation by a Series of First Row Transition Metal Tris(2-Pyridylmethyl)Amine Complexes. *Inorg. Chem.* **2012**, *51*, 4694−4706.

(58) Cardenal, A. D.; Maity, A.; Gao, W. Y.; Ashirov, R.; Hyun, S. M.; Powers, D. C. Iodosylbenzene Coordination Chemistry Relevant to Metal-Organic Framework Catalysis. *Inorg. Chem.* **2019**, *58*, 10543−10553.

(59) Menges, F. *Spectragryph - Optical Spectroscopy Software*, 2019.

(60) Stoll, S.; Schweiger, A. *EasySpin, a Comprehensive Software Package for Spectral Simulation and Analysis in EPR*, 2005.

(61) Molton, F. Simultispin: A Versatile Graphical User Interface for the Simulation of Solid-State Continuous Wave EPR Spectra. *Magn. Reson. Chem.* **2020**, *58*, 718−726.

(62) Petasis, D. T.; Hendrich, M. P. Quantitative Interpretation of Multifrequency Multimode EPR Spectra of Metal Containing Proteins, Enzymes, and Biomimetic Complexes. *Methods Enzymol.* **2015**, *563*, 171−208.

(63) Wojdyr, M. Fityk: A General Purpose Peak Fitting Program. *J. Appl. Crystallogr.* **2010**, *43*, 1126−1128.

https://doi.org/10.1021/acs.inorgchem.1c00684
Inorg. Chem. XXXX, XXX, XXX−XXX